Original Article

Diluted aqueous extract of heat-not-burn tobacco product smoke causes less oxidative damage in fibroblasts than conventional cigarette

Qinying Lyu,[1] Li Jiang,[1] Hao Zheng,[1] Shotaro Hayashi,[1,2] Kotaro Sato,[1,3] and Shinya Toyokuni[1,4,*]

[1]Department of Pathology and Biological Responses, [2]Department of Obstetrics and Gynecology, and [3]Department of Oral and Maxillofacial Surgery, Nagoya University Graduate School of Medicine, 65 Tsurumai-cho, Showa-ku, Nagoya 466-8550, Japan
[4]Center for Low-temperature Plasma Sciences, Nagoya University, Furo-cho, Chikusa-ku, Nagoya 484-8601, Japan

(Received 28 September, 2021; Accepted 21 November, 2021; Released online in J-STAGE as advance publication 25 January, 2022)

Smoke from conventional cigarettes (C-cigarettes) contains various reactive oxygen species and toxic chemicals, which potentially cause oxidative damage not only to airways but also to the whole body, leading eventually to diseases, including emphysema, advanced atherosclerosis, and cancer. Many heat-not-burn tobacco products (HTPs) have been commercialized recently in Japan to maintain the smoking population by advertising that HTPs are less toxic. However, there were few studies reported from neutral organizations whether HTPs are indeed less damaging. To evaluate the potential capacity of HTPs to induce oxidative stress, we here compared two different HTPs with two types of C-cigarettes, using human fibroblast IMR90SV cells and 5% aqueous extracts in 10-ml phosphate-buffered saline (50-ml smoke/10 s). HTPs exhibited significantly lower oxidative toxicity in comparison to C-cigarettes. Whereas C-cigarettes induced ferroptosis in fibroblasts, the effects of HTPs were significantly reduced by measuring the levels of peroxides, pro-inflammatory cytokine expression, autophagy, catalytic Fe(II) and 8-hydroxy-2'-deoxyguanosine. Notably, major portions of C-cigarettes-induced pathogenic responses were inhibited by catalase. However, HTPs still induced p62 autophagy-adaptor at 5%-dilution and caused lethal effects to fibroblasts with undiluted solution. In conclusion, HTPs smoke *per se* can be toxic despite less toxicity in comparison to C-cigarettes, which warrants further investigation.

***Key Words*: heat-not-burn tobacco product, hydrogen peroxide, oxidative stress, autophagy, ferroptosis**

Conventional combustion-type cigarette (C-cigarette) smoke contains numerous toxic and carcinogenic chemicals, including various reactive oxygen species (ROS),[1] leading eventually to diseases, such as chronic pulmonary diseases,[2] cancer,[3] diabetes,[4] neurodegeneration,[5,6] and cardiovascular diseases[7,8] after long-time use. Hydrogen peroxide (H_2O_2) is an important ROS which is physiologically generated in cells from superoxide (O_2^-) or molecular oxygen (O_2).[9] Appropriate intracellular H_2O_2 level facilitates the basic signaling pathway whereas excess H_2O_2 is associated with various pathologies through oxidative stress.[10,11] High oxidative stress causes lipid peroxidation, protein damage and DNA modification/strand breaks,[12,13] stimulating immunogenic responses.[14,15] Damaged proteins would be degraded to protect cells from regulated cell death (RCD).[16] Ubiquitin-proteasome system (UPS) and autophagy are the two major systems to maintain cellular proteostasis.[17] p62 (SQSTM1) is a multifunctional protein which delivers damaged proteins to autophagic process. Nuclear factor-κB (NF-κB)[18] has been reported as an upstream transcription factor of *p62* expression under oxidative stress.[19] NF-κB/p62 signaling plays a critical role in regulating autophagy and cell survival.[20]

Recently, it was reported that C-cigarette smoke causes ferritin-selective autophagy (ferritinophagy) and ferroptosis in epithelial cells of human respiratory system.[21,22] Ferroptosis is a catalytic Fe(II)-dependent RCD accompanied by phospholipid peroxidation, [23,24] which may be closely associated with autophagy[25] and carcinogenesis.[26–28] Stable free radicals in the tar phase of C-cigarette have high potential for redox recycling and oxidative reactions[29] and hydroxyl radicals generated by synergistic reaction catalyzed by Fe(II) can react with DNA to produce mutagenic 8-hydroxy-2'-deoxyguanosine (8-OHdG),[30,31] promoting carcinogenesis not only through genetic but also epigenetic mechanisms.[1] To attract and maintain the smoking population, various electronic cigarettes, including heat-not-burn tobacco products (HTPs), have been launched recently.[32] HTP consumptions have been increasing rapidly in developed countries, such as Japan and the United States.[33,34]

HTPs reportedly reduced harmful particles by 72.4–86.2% in its smoke in comparison to C-cigarettes.[35,36] However, there were few studies reported from neutral academic organizations whether HTPs are indeed less damaging.[37] Here, we studied the differences in the biological effects on cultured fibroblasts, from the viewpoint of autophagy, inflammation, and oxidative stress/damage between aqueous extract of HTPs and that of C-cigarettes. Our study revealed that HTPs are less toxic than C-cigarettes at 5%-dilution but that HTPs are still cytotoxic without dilution.

Materials and Methods

Cell culture. SV40-transformed human lung fibroblast cell line IMR90SV was obtained from the Riken Cell Bank (Ibaraki, Japan). The cells were grown in RPMI-1640 medium (Wako, Osaka, Japan) with 10% fetal bovine serum (Biowest, Nuaillé, France) and 1% antibiotic-antimycotic solution (Invitrogen, Carlsbad, CA) and maintained in a humidified incubator at 37°C with 5% CO_2.

*To whom correspondence should be addressed.
E-mail: toyokuni@med.nagoya-u.ac.jp

doi: 10.3164/jcbn.21-134

Table 1. Commercial C-cigarettes and HTPs used for aqueous smoke extract preparation

Smoke extract solution	Brands
CSE #1	Wakaba, JT; Tokyo, Japan
CSE #2	Peace, JT; Japan
HTPE #1	glo™ (KENT Neostiks for glo); British American Tobacco Japan, Ltd.; Tokyo, Japan
HTPE #2	iQOS (Marlboro, regular), Philip Morris Japan; Tokyo, Japan

C-cigarette, conventional cigarette; CSE, C-cigarette smoke extract; HTP, heat-not-burn tobacco product; HTPE, HTP smoke extract.

Preparation of C-cigarette smoke extract (CSE) and HTP smoke extract (HTPE). Smoke from one unit of C-cigarette or HTP was bubbled into 10 ml Dulbecco's phosphate-buffered saline (D-PBS, Wako) at a speed of 10 s/50 ml pumping. CSE/HTPE solution was filtered (0.22 μm Milex-GS; SLGS033SB) to sterilize and remove insoluble particles. Commercial C-cigarettes and HTPs used are listed in Table 1. Smoke from one C-cigarettes or HTP in 10 ml D-PBS was considered as 100% CSE/HTPE solution. 100% CSE or HTPE was diluted with an appropriate culture medium to make the indicated final concentration (v/v), depending on the experimental conditions. Condensed extract (200%) was generated by bubbling smoke from 2 units of HTPs directly into 10 ml culture medium, followed sterilization. Thereafter, 200% condensed extract was diluted with the same volume of culture medium to generate 100% HTPE.

Cell viability and cytotoxicity assay. Five thousand cells/well were seeded in 96-well plates (Cat. #167008; Thermo Fisher Scientific, Waltham, MA) and incubated overnight. Cells were then treated with CSE or HTPE according to each condition of the protocol. After treatment, cell viability was examined by the cell count reagent SF (Cat. #07553; Nacalai Tesque, Kyoto, Japan) according to the manufacture's protocol. The cytotoxicity was determined by release of LDH into the media by cytotoxicity LDH assay kit (Cat. #CK12; Dojindo, Kumamoto, Japan). Cell death was visualized by SYTOX green nucleic acid staining (Cat. #S7020; Thermo Fishier Scientific), a chromosome counterstain that only penetrates the membrane of dead cells. Nuclei were counterstained with Hoechst 33342 (Cat. #346-07951; Dojindo).

Quantitative real-time PCR. Total RNA was extracted by RNeasy Plus Mini Kit (Cat. #74134; QIAGEN, Hilden, Germany). Double-stranded cDNA were generated with SuperScript III First-Strand Synthesis System for RT-PCR (Cat. #18080-051; Invitrogen). Quantitative real-time PCR were performed by Bio-Rad CFX96 Touch Real-Time PCR Detection System using Platinum™ SYBR™ Green qPCR SuperMix-UDG (Cat. #11733-038; Invitrogen), and mRNA levels were quantified with the following primers: *TNF-α* (forward: 5'-CTCTTCTGC CTGCTGCACTTTG-3' and reverse: 5'-ATGGGCTACAGG CTTGTCACTC-3'), *IL1-α* (forward: 5'-GCGACACTGTTCGTG TTGTC-3' and reverse: 5'-GGCAGTATTCAAGCCTCCCA-3'), *IFN-β* (forward: 5'-GCGACACTGTTCGTGTTGTC-3' and reverse: 5'-GGCAGTATTCAAGCCTCCCA-3'), and *GAPDH* (forward: 5'-CTGACTTCAACAGCGACACC-3' and reverse: 5'-TAGCCAAATTCGTTGTCATACC-3'). Gene expression was normalized to *GAPDH,* using $\Delta\Delta Ct$ method.

Immunohistochemistry (IHC) analysis for paraffin-embedded specimens. Treated cells were collected and fixed with 4% (w/v) paraformaldehyde (Alfa Aesar, Thermo Fisher Scientific, Waltham, MA) to make paraffin-embedded sections. IHC staining was performed on paraffin section with Leica Bond Max automated system (Leica, Bannockburn, IL). 8-OHdG (Cat. #BS-1278R; Bioss Antibodies, Woburn, MA) and HNEJ-2[38] primary antibodies were used (1:2,000 dilution). Images were obtained by Olympus BX53 microscope and analyzed with ImageJ (https://imagej.nih.gov/ij/).

Immunocytochemistry (ICC) analysis for cultured cells. Treated cells were fixed with 4% (w/v) paraformaldehyde on glass bottom chamber culture slides. Following incubation with 0.1% (v/v) Triton X100 to enhance membrane permeability and blocking with 3% (w/v) bovine serum albumin (BSA), cells were incubated either with primary antibody against NF-κB p65 (Cat. #8242, 1:2,000 dilution; Cell Signaling Technology, Danvers, MA) or SQSTM1/p62 (Cat. #D5L7G, 1:1,000 dilution; Cell Signaling Technology) overnight at 4°C. The cells were then washed with D-PBS and stained with secondary antibodies and DAPI-Fluoromount-G. Images were captured through Zeiss confocal microscope (LSM880; Carl Zeiss, Oberkochen, Germany).

Immunoblotting. Treated cells were homogenized in ice-cold radioimmunoprecipitation (RIPA) buffer after treatment. Protein of 10 μg was electrophoresed in SDS-polyacrylamide gel and was transferred to polyvinylidene fluoride membranes (Cat. #1620117; Bio-Rad). The membranes were blocked with 5% (w/v) skim-milk in Tris-buffered saline with Tween 20 (TBST), followed by immunostaining either with antibodies against SQSTM1/p62 (Cat. #D5L7G, 1:1,000 dilution; Cell Signaling Technology), LC3B (Cat. #D11, 1:1,000 dilution; Cell Signaling Technology), LAMP1 (Cat. #D2D11, 1:1,000 dilution; Cell Signaling Technology), ferritin heavy (H) chain (Cat. #ab65080, 1:1,000 dilution; Abcam, Cambridge, UK), ferritin light (L) chain (Cat. #ab69090, 1:1,000 dilution; Abcam) or β-actin (Cat. #clone AC-15, 1:5,000 dilution; Sigma-Aldrich, St. Louis, MO).

Time-lapse fluorescent imaging of H_2O_2. H_2O_2 production was tracked, using genetically encoded red fluorescent probe HyPerRed (plasmid #48249, a gift from Dr. Vsevolod Belousov).[39] IMR90SV cells were incubated at 37°C in FluoroBrite™ DMEM (Cat. #A1896701; Gibco, Amarillo, TX). Time-lapse fluorescence imaging was obtained by BIOREVO BZ-9000 KEYENCE fluorescent microscope, using PBS as a negative control. The fluorescence intensity was analyzed with ImageJ software.

Calcein-AM labile iron pool (LIP) assay. IMR90SV cells (3×10^5) were seeded in 6-well plates and incubated overnight at 37°C with 5% CO_2. Cells were then incubated with 0.1 μM calcein-AM (Cat. #C396; Dojindo) for 30 min at 37°C in FluoroBrite™ DMEM (Cat. #A1896701; Gibco). After calcein loading and 4-h treatment either by CSE or HTPE, cells were washed with PBS and filled with new FluoroBrite™ DMEM. Fluorescent intensity was quantified with flow cytometry and the fluorescence images was obtained by BIOREVO BZ-9000 KEYENCE fluorescent microscope.

Statistical analysis. Statistical differences were analyzed by Student's *t* test or one-way ANOVA, followed by Tukey's multiple comparison test. Analysis was performed with Prism 9.0 software (GraphPad Software, San Diego, CA). Significance was defined as $p<0.05$.

Results

HTPE induces less damage to IMR90SV fibroblasts in comparison to CSE. IMR90SV cells were exposed either to CSE or HTPE at various concentrations for 24 h. Cell viability was significantly reduced by CSE treatment in a time- and concentration-dependent manner (Fig. 1A and B), consistent with a significant increase in cytotoxicity after CSE treatment in a concentration-dependent manner (Fig. 1C and E). In contrast, HTPE at 5%-dilution affected neither cell viability nor cytotoxicity of IMR90SV (Fig. 1A–C). However, HTPE of 100% (undiluted) or 200% was significantly cytotoxic (Fig. 1D). Hereafter, 5%-dilution of CSE/HTPE was used in all the experiments

doi: 10.3164/jcbn.21-134

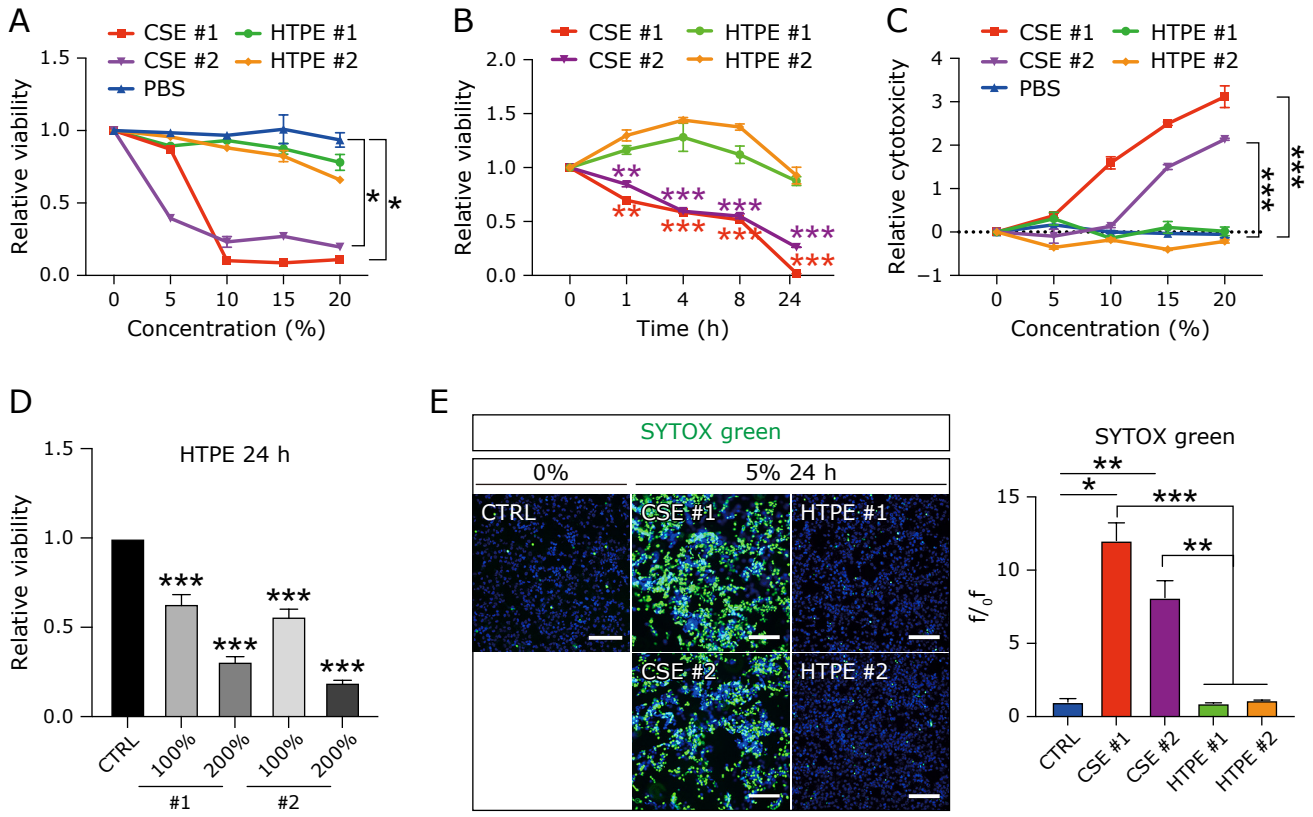

Fig. 1. Suppression of cell growth and induction of cell death by CSE but not by HTPE after dilution of the aqueous extract. (A, B) Proliferation of IMR90SV fibroblasts was suppressed with CSE treatment in a concentration- and time-dependent manner but not with HTPE treatment after dilution. Cell viability was assessed with WST-8 assay at 24 h unless otherwise specified. 5%-Dilution was thereafter used unless otherwise specified. (C) CSE caused cellular damage and death with increasing concentration whereas HTPE did not up to 20%-dilution. Cytotoxicity was assessed by LDH assay. (D) HTPE of 100% (v/v) or 200% (v/v) caused cellular damage after 24 h treatment. (E) After treatment with 5% CSE or HTPE for 24 h, cell death was assessed with SYTOX green (bar = 200 μm; based on 3 independent experiments; mean ± SEM; *p<0.05, **p<0.01, ***p<0.001. CSE, conventional cigarette smoke extract; HTPE, heat-not-burn tobacco product smoke extract; PBS, phosphate-buffered saline. Refer to text and Table 1 for details.

unless otherwise specified to compare the difference for a period of 24 h.

CSE and HTPE differentially induces overexpression of pro-inflammatory cytokines and NF-κB/p62 regulated autophagy in IMR90SV fibroblasts. Pro-inflammatory cytokines are a broad range of small proteins important for signaling necrotic RCD.[40] mRNA levels of *TNF-α*, *IFN-β*, and *IL1-α* were significantly elevated 4 h after CSE treatment whereas HTPE induced no significant increase in all the three cytokines examined (Fig. 2A–C). TNF-α, Interleukin-1 and oxidative stress play a role in activating the transcription factor NF-κB family.[18,41] ICC analysis revealed that NF-κB translocated from cytoplasm to nucleus 8 h not only after CSE but also after HTPE treatment (Fig. 2D and Supplemental Fig. 1*). p62 (SQSTM1) is a multifunctional protein associated with autophagy and is transcriptionally regulated by NF-κB.[42] Both ICC and immunoblot analyses revealed increased p62 expression after CSE and HTPE treatments (Fig. 2D, F, and G). However, both nuclear NF-κB and p62 induced by HTPE treatment was significantly lower than those by CSE treatment. LC3-II is a protein associated with autophagosomal membrane and increased LC3-II/LC3-I ratio reflects up-regulated activity of autophagy.[17,19] LC3-II/LC3-I ratio was significantly elevated after CSE treatment whereas the ratio revealed no alteration after HTPE treatment (Fig. 2E and Supplemental Fig. 2*). Autophagosomes fuse with lysosome to form autolysosome which facilitates degradation of damaged proteins[17]. Lysosomal membrane protein, LAMP1, assessed by immunoblot analysis was increased simultaneously with LC3-II after CSE treatment but not after HTPE treatment (Fig. 2F and G).

Different biological responses between CSE and HTPE exposure at least partially depends on H_2O_2. ROS have a potential to cause injuries in the airway and the release of damage-associated molecular patterns which can lead to diseases such as chronic obstructive pulmonary diseases and asthma.[21,43] To study the ROS production *de novo* in CSE- or HTPE-treated IMR90SV cells, we introduced a genetically encoded indicator HyPerRed[39] into IMR90SV cells to track H_2O_2 levels continuously. Immediate and prominent H_2O_2 increase was observed in IMR90SV cells after CSE exposure. However, intracellular H_2O_2 elevation after HTPE exposure was much lower though HTPE#1 showed a significant increase (Fig. 3A). To evaluate whether H_2O_2 contributes as a major factor to make differences in cellular damage and inflammatory response between CSE and HTPE treatment, catalase (CAT), an enzyme to catalyze H_2O_2 degradation, was used prior to the CSE treatment. H_2O_2 as a final concentration of 100 μM was used as a positive control. CAT significantly inhibited CSE-induced cell death as measured by WST-8 assay (Fig. 3B). To further investigate whether inflammatory responses and autophagy can be suppressed by H_2O_2 depletion, we added CAT to IMR90SV fibroblasts with the two types of CSEs. Quantitative real-time PCR results of mRNA demonstrated that CSE-induced *TNF-α*, *IFN-β*, and *IL1-α* overexpression was all significantly inhibited by CAT (Fig. 3C–E).

In order to investigate whether p62/NF-κB-regulated autophagy can be attenuated as well by H_2O_2 degradation, we

*See online. https://doi.org/10.3164/jcbn.21-134

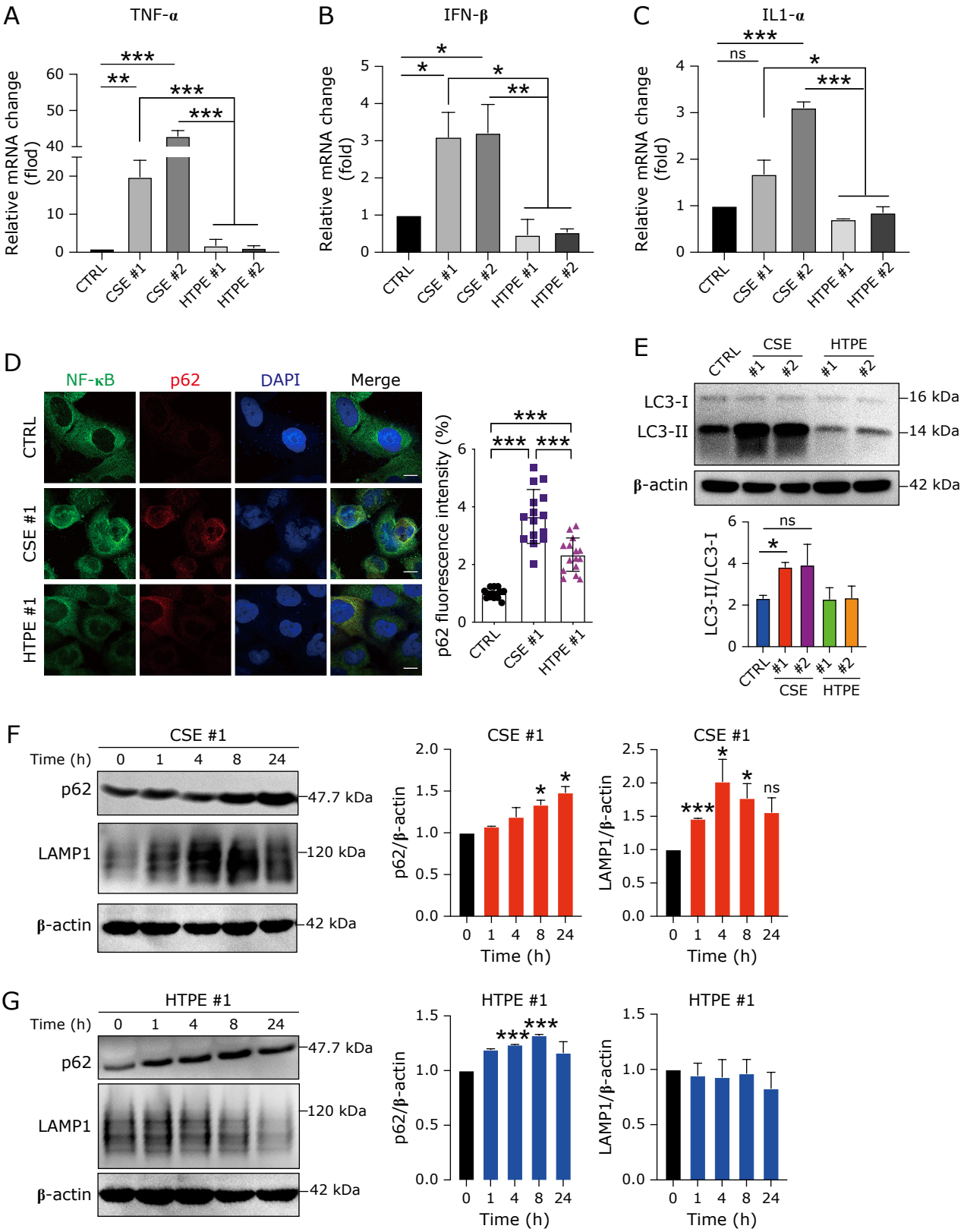

Fig. 2. CSE and HTPE induces NF-κB activation and p62-regulated autophagy. (A, B, C) IMR90SV cells were treated with CSE (5%) or HTPE (5%) for 4 h, and the mRNA levels of *TNF-α*, *IFN-β*, and *IL1-α* were assessed with quantitative real-time PCR analysis. (D) IMR90SV cells were treated with 5% CSE or 5% HTPE for 8 h. Nuclear NF-κB and cytoplasmic p62 increased in both CSE- and HTPE-treated IMR90SV cells. Results were obtained with immunocytochemical analysis (bar = 13 μm). (E, F, G) CSE triggered p62-regulated autophagy more intensely than HTPE. Expression of p62, LC3B and LAMP1 was increased. Protein levels were examined by immunoblot analysis (mean ± SEM; *p<0.05, **p<0.01, ***p<0.001).

doi: 10.3164/jcbn.21-134

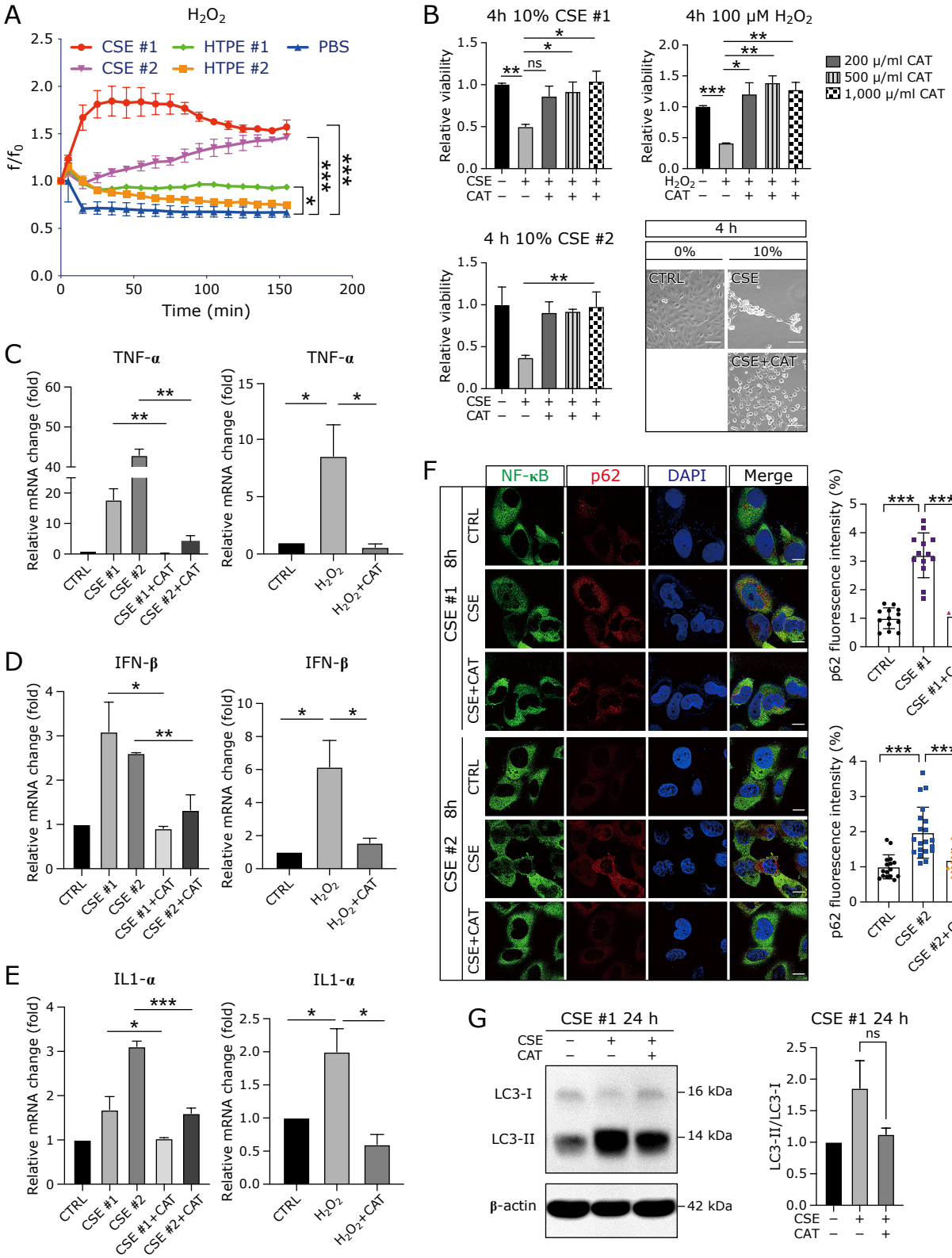

Fig. 3. H_2O_2 is a major responsible chemical for oxidative damage and inflammatory response of IMR90SV fibroblasts exposed to CSE. (A) Time-lapse alteration of intracellular H_2O_2 by HyPerRed florescence in response to 5% CSE, 5% HTPE or PBS. Data was obtained by time-lapse microscopy at 10-min interval. CSE treatment significantly increased intracellular H_2O_2 level in comparison to HTPE or PBS group. (B) Catalase (CAT; 200, 500 or 1,000 unit/ml) was added prior to 10% CSE or 100 μM H_2O_2 treatment. WST-8 measurements and phase-contrast microscopic images are shown (bar = 100 μm). (C, D, E) The cells were treated with 5% CSE or 100 μM H_2O_2 in the presence or absence of CAT (500 unit/ml) for 4 h. Relative mRNA level of *TNF-α*, *IFN-β*, and *IL1-α* were assessed by quantitative real-time PCR analyses. (F) CAT was added to IMR90SV cells 30 min before 8 h CSE treatment (5%). Confocal images reveal the significant increase in nucleic NF-κB and cytoplasmic p62 levels elevated by CSE, which were repressed by co-treatment with CAT (bar = 13 μm). (G) IMR90SV cells were treated with 5% CSE with or without CAT (500 unit/ml) for 24 h. Protein levels of LC3B-I/II were analyzed with immunoblotting. β-actin was used as an internal control (means ± SEM; *p<0.05, **p<0.01, ***p<0.001).

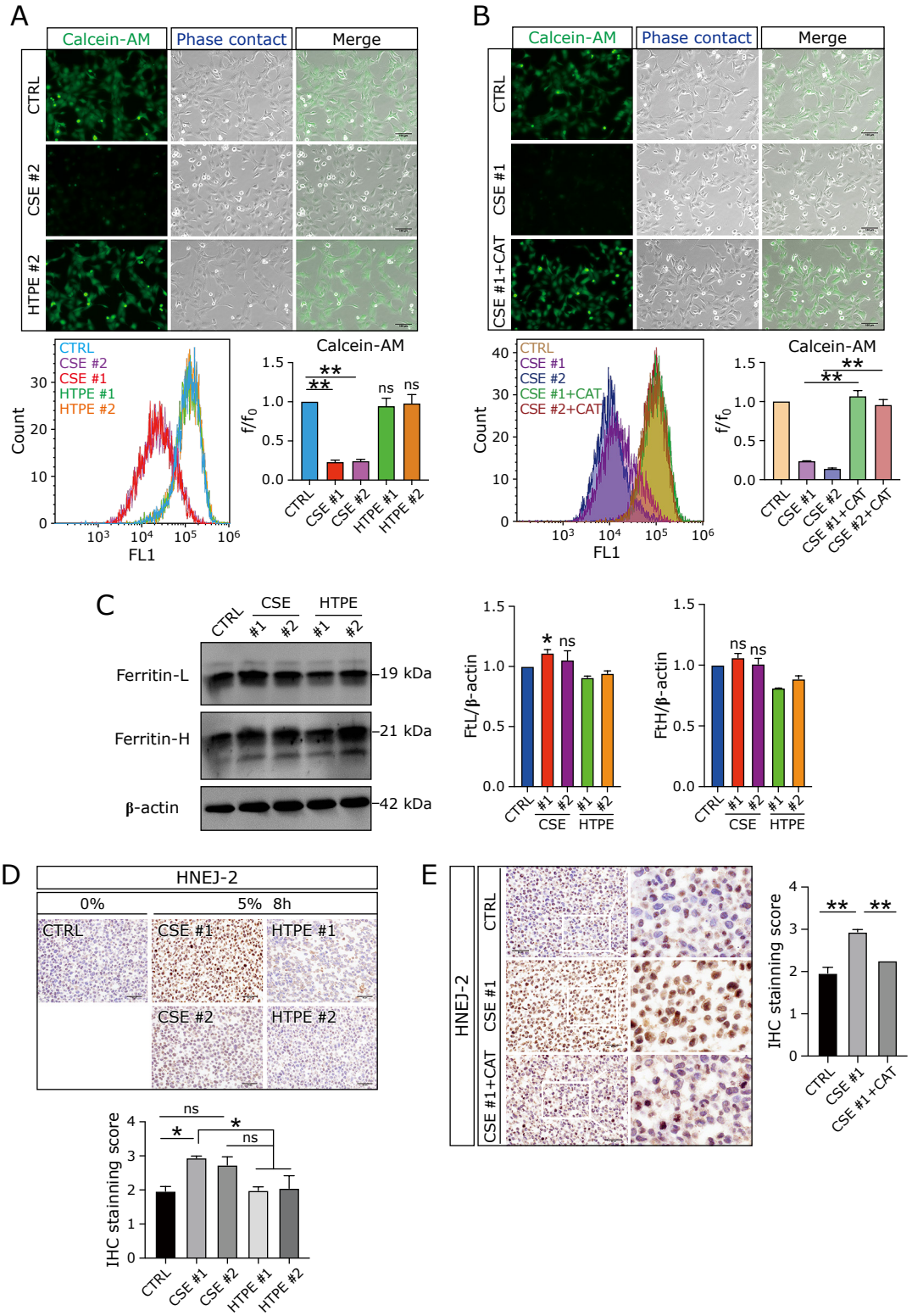

Fig. 4. CSE but not HTPE significantly increases intracellular catalytic Fe(II), causing ferroptosis. (A) IMR90SV cells were treated with CSE (5%) or HTPE (5%) for 4 h, catalytic Fe(II) as labile iron pool (LIP) quantified by Calcein-AM assay was significantly increased by CSE treatment in comparison to the control group whereas HTPE did not increase LIP (bar = 100 μm). (B) IMR90SV cells were treated with 5% CSE with or without CAT (500 unit/ml) for 4 h, followed by analyses of LIP as described. CAT was effective (bar = 100 μm). (C) Protein was extracted for immunoblot analyses after 4 h CSE (5%) or HTPE (5%) treatment. Expression of ferritin-H and ferritin-L was increased only in CSE-treated groups, confirming the increase in intracellular iron. (D, E) IMR90SV cells were treated with CSE (5%) or HTPE (5%) for 8 h, where significant lipid peroxidation with HNEJ-2 antibody was detected only in CSE treatment groups, confirming ferroptosis. Increased lipid peroxidation by CSE #1 was significantly suppressed by additional CAT co-incubation (bar = 50 μm; data were taken from 3 independent experiments; mean ± SEM; *p<0.05, **p<0.01). CAT, catalase; LIP, labile iron pool. Refer to text for details.

doi: 10.3164/jcbn.21-134

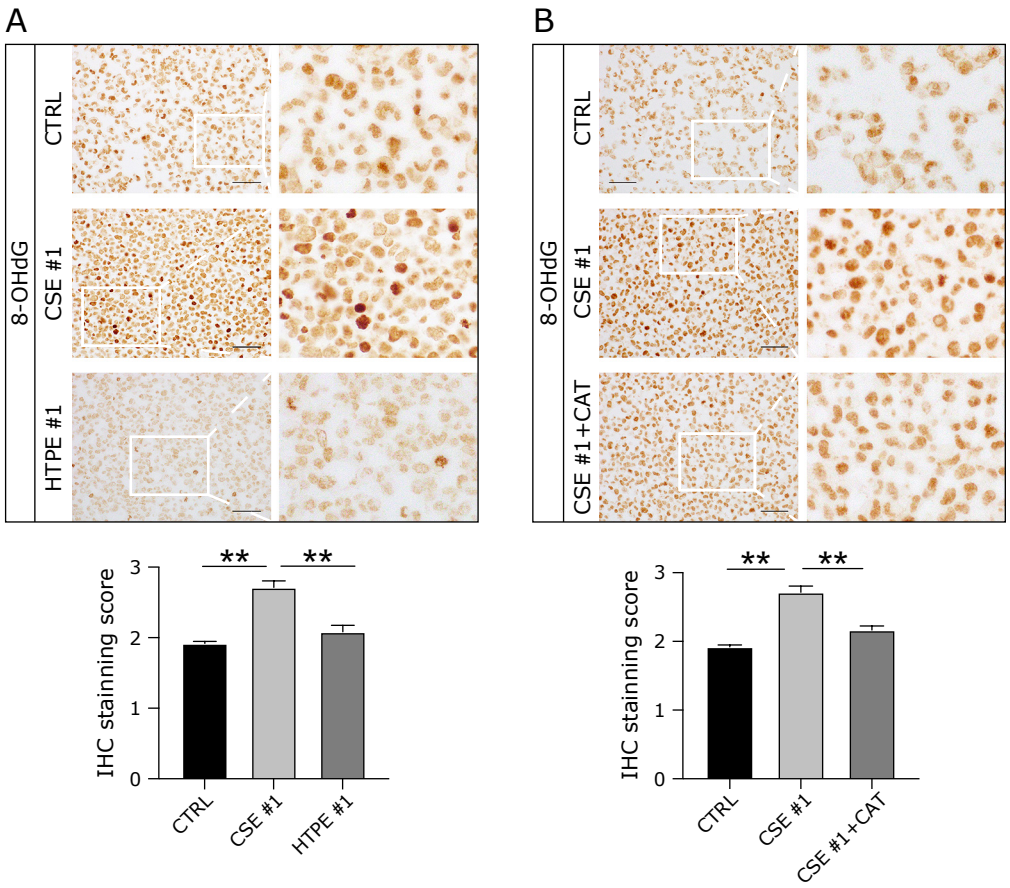

Fig. 5. CSE but not HTPE induces oxidative DNA damage, which is rescued by CAT. (A) IMR90SV cells were treated with CSE (5%) or HTPE (5%) for 8 h. Significantly increased 8-OHdG was detected in CSE treatment group in comparison to the control or HTPE treatment group. (B) IMR90SV cell were treated with 5% (v/v) CSE with or without additional CAT (500 unit/ml) for 8 h. Immunohistochemical analysis exhibited significantly decreased 8-OHdG level in CSE treatment group with additional CAT in comparison to CSE treatment group without CAT (bar = 50 μm; means ± SEM; $^{**}p<0.01$). CAT, catalase; 8-OHdG, 8-hydroxy-2'-deoxyguanosine.

performed immunoblot and ICC analyses, which showed that up-regulated p62 protein level, LC3-II/LC3-I ratio and nuclear NF-κB after CSE exposure were significantly suppressed by CAT (Fig. 3F, G, and Supplemental Fig. 3*).

CSE but not HTPE significantly expands LIP and lipid peroxidation. Maintenance of LIP homeostasis is important for cells because Fe(II) but not Fe(III) plays a role in in oxidation-reduction reactions.[44] Fe(III) is practically not soluble at neutral pH and is used to store iron in ferritin.[45,46] Excess intracellular catalytic Fe(II) level has a potential to induce ferroptosis, an iron-dependent form of RCD,[23,24,47] which is associated with various pathological conditions.[48] Calcein-AM assay is widely used to analyze LIP as calcein fluorescence is quenched following iron chelation.[49] Calcein-AM-loaded IMR90SV cells were treated either with CSE or HTPE, followed by analyses after 4 h-incubation. Both flow cytometry and microscopic analyses showed significantly increased LIP in the CSE group whereas HTPE group even at 100% or 200% showed no significant alteration of LIP in comparison to the control group (Fig. 4A, Supplemental Fig. 4*, and Supplemental Fig. 5*). Expanded LIP by CSE was significantly repressed by CAT (Fig. 4B and Supplemental Fig. 4B*). Expanded LIP was consistent with ferritin induction 4 h after CSE exposure (Fig. 4C).

We selected 4-hydroxy-2-nenenal (HNE) to evaluate lipid peroxidation with a monoclonal antibody produced against HNE-modified proteins.[38] IHC results exhibited that CSE, especially #1, induced more HNE production in comparison to the HTPE (Fig. 4D), demonstrating the induction of ferroptosis after CSE exposure. HNE production by CSE was significantly inhibited by CAT (Fig. 4E).

CSE but not HTPE induces oxidative DNA damage. IMR90SV fibroblasts were treated either with CSE or HTPE for 8 h. IHC analysis revealed increased 8-OHdG level after CSE treatment but not after HTPE treatment (Fig. 5A). Elevated 8-OHdG level by CSE was significantly reduced by CAT (Fig. 5B).

Discussion

We evaluated the cytotoxic effects of HTPE on human lung fibroblasts in comparison to CSE based on a neutral academic standpoint. At the optimal experimental condition of 5%-dilution of the smoke extracts, HTPE was significantly less toxic than CSE in all the indicators measured in the present experiment. HTPs revealed a significant reduction of intracellular H_2O_2 production in comparison to CSE at 5%-dilution. However, HTPE still activated NF-κB/p62 system, initiating autophagic processes, which means that HTPs still disturbs p62 homeostasis. Unregulated p62 homeostasis is potentially pathogenic and tumorigenic.[50] Furthermore, HTPE was certainly cytotoxic if not diluted. Because we have used an apparatus to mimic human smoking to prepare smoke extract, airway cells would be exposed to ~100% HTPE when people smoke HTP. We have to fully recognize that HTPE is still cytotoxic enough and that advertising less toxicity of HTPE than CSE is possibly an overstatement.

In the present experiment, we could obtain further insights

*See online. https://doi.org/10.3164/jcbn.21-134

into the CSE-induced cytotoxicity. RCD form in CSE-exposed fibroblasts was ferroptosis with increased lipid peroxidation as evaluated by HNE and 8-OHdG.[51,52] Strikingly, both H_2O_2 and catalytic Fe(II) were significantly increased at early hours after CSE exposure such as 0.5–4 h, especially with H_2O_2 of CSE#1 as early as 20 min, with continuous monitoring. One of the HTPEs also induced H_2O_2 production though the level was significantly lower than that of CSEs. The increased H_2O_2 production should have promoted intracellular Fenton reaction[53] to cause oxidative stress and further chemical reactions. This was indeed accompanied by inflammatory responses as evaluated by the overexpression of TNF-α, IFN-β, and IL1-α.[18,41] We observed that this ferroptosis was preceded by autophagic process, as in the case of non-thermal plasma activated lactate-induced ferroptosis of malignant mesothelioma cells.[54,55]

Of note, most of the pathologies we observed in the present experiments could be significantly suppressed in the presence of additional catalase. Therefore, catalase itself, its mimic or catalase inducer may help to prevent the side effects of C-cigarettes. The limitation of the current study is that we used only the aqueous extract. Accordingly, we may miss some pathologic effects of lipophilic or particulate molecules[35,36] and their combined effects thereby.

In conclusion, HTPE can be less toxic than CSE at the optimal experimental condition. However, we should be aware that HTPE *per se* with no dilution is toxic enough to cause various pathologies. Further studies are warranted on HTPs because the HTPs smokers are increasing and specific diseases, such as E-cigarette use-associated lung injury, are also reported.[56]

Acknowledgments

The authors thank Dr. Vsevolod Belousov for providing a plasmid, pC1-HyPer-Red, genetically encoded hydrogen peroxide indicator with red fluorescence. This work was supported, in part, by JST CREST (Grant Number JPMJCR19H4), JSPS KAKENHI (Grant Number JP19H05462 and JP20H05502) and Research Grant of the Princess Takamatsu Cancer Research Fund (19-251).

Abbreviations

BSA	bovine serum albumin
CAT	catalase
C-cigarette	conventional cigarette
CSE	C-cigarette smoke extract
HNE	4-hydroxy-2-nonenal
HTP	heat-not-burn tobacco product
HTPE	heat-not-burn tobacco product smoke extract
ICC	immunocytochemistry
IHC	immunohistochemistry
LIP	labile iron pool
NF-κB	nuclear factor-κB
PBS	phosphate-buffered saline
RCD	regulated cell death
RIPA	radioimmunoprecipitation
ROS	reactive oxygen species
TBST	Tris-buffered saline with Tween 20
UPS	ubiquitin-proteasome system

Conflict of Interest

No potential conflicts of interest were disclosed.

References

1 Valavanidis A, Vlachogianni T, Fiotakis K. Tobacco smoke: involvement of reactive oxygen species and stable free radicals in mechanisms of oxidative damage, carcinogenesis and synergistic effects with other respirable particles. *Int J Environ Res Public Health* 2009; **6**: 445–462.
2 Young RP, Hopkins RJ, Christmas T, Black PN, Metcalf P, Gamble GD. COPD prevalence is increased in lung cancer, independent of age, sex and smoking history. *Eur Respir J* 2009; **34**: 380–386.
3 Doll R, Hill AB. Lung cancer and other causes of death in relation to smoking; a second report on the mortality of British doctors. *Br Med J* 1956; **2**: 1071–1081.
4 Haire-Joshu D, Glasgow RE, Tibbs TL. Smoking and diabetes. *Diabetes Care* 1999; **22**: 1887–1898.
5 Fratiglioni L, Wang HX. Smoking and Parkinson's and Alzheimer's disease: review of the epidemiological studies. *Behav Brain Res* 2000; **113**: 117–120.
6 Cataldo JK, Prochaska JJ, Glantz SA. Cigarette smoking is a risk factor for Alzheimer's disease: an analysis controlling for tobacco industry affiliation. *J Alzheimers Dis* 2010; **19**: 465–480.
7 Lakier JB. Smoking and cardiovascular disease. *Am J Med* 1992; **93**: 8S–12S.
8 Ockene IS, Miller NH. Cigarette smoking, cardiovascular disease, and stroke: a statement for healthcare professionals from the American Heart Association. American Heart Association Task Force on Risk Reduction. *Circulation* 1997; **96**: 3243–3247.
9 Winterbourn CC. Reconciling the chemistry and biology of reactive oxygen species. *Nat Chem Biol* 2008; **4**: 278–286.
10 Veal EA, Day AM, Morgan BA. Hydrogen peroxide sensing and signaling. *Mol Cell* 2007; **26**: 1–14.
11 Schieber M, Chandel NS. ROS function in redox signaling and oxidative stress. *Curr Biol* 2014; **24**: R453–R462.
12 Toyokuni S. Reactive oxygen species-induced molecular damage and its application in pathology. *Pathol Int* 1999; **49**: 91–102.
13 Toyokuni S, Akatsuka S. Pathological investigation of oxidative stress in the post-genomic era. *Pathol Int* 2007; **57**: 461–473.
14 Møller P, Folkmann JK, Forchhammer L, *et al*. Air pollution, oxidative damage to DNA, and carcinogenesis. *Cancer Lett* 2008; **266**: 84–97.
15 Cross CE, Halliwell B, Borish ET, *et al*. Oxygen radicals and human disease. *Ann Intern Med* 1987; **107**: 526–545.
16 Mizushima N. Autophagy: process and function. *Genes Dev* 2007; **21**: 2861–2873.
17 Liu WJ, Ye L, Huang WF, *et al*. p62 links the autophagy pathway and the ubiqutin-proteasome system upon ubiquitinated protein degradation. *Cell Mol Biol Lett* 2016; **21**: 29.
18 Lingappan K. NF-κB in oxidative stress. *Curr Opin Toxicol* 2018; **7**: 81–86.
19 Song C, Mitter SK, Qi X, *et al*. Oxidative stress-mediated NFκB phosphorylation upregulates p62/SQSTM1 and promotes retinal pigmented epithelial cell survival through increased autophagy. *PLoS One* 2017; **12**: e0171940.
20 Duran A, Linares JF, Galvez AS, *et al*. The signaling adaptor p62 is an important NF-kappaB mediator in tumorigenesis. *Cancer Cell* 2008; **13**: 343–354.
21 Yoshida M, Minagawa S, Araya J, *et al*. Involvement of cigarette smoke-induced epithelial cell ferroptosis in COPD pathogenesis. *Nat Commun* 2019; **10**: 3145.
22 Park EJ, Park YJ, Lee SJ, Lee K, Yoon C. Whole cigarette smoke condensates induce ferroptosis in human bronchial epithelial cells. *Toxicol Lett* 2019; **303**: 55–66.
23 Stockwell BR, Friedmann Angeli JP, Bayir H, *et al*. Ferroptosis: a regulated cell death nexus linking metabolism, redox biology, and disease. *Cell* 2017; **171**: 273–285.
24 Toyokuni S, Yanatori I, Kong Y, Zheng H, Motooka Y, Jiang L. Ferroptosis at the crossroads of infection, aging and cancer. *Cancer Sci* 2020; **111**: 2665–2671.
25 Gao M, Monian P, Pan Q, Zhang W, Xiang J, Jiang X. Ferroptosis is an autophagic cell death process. *Cell Res* 2016; **26**: 1021–1032.
26 Toyokuni S, Ito F, Yamashita K, Okazaki Y, Akatsuka S. Iron and thiol redox signaling in cancer: an exquisite balance to escape ferroptosis. *Free Radic Biol Med* 2017; **108**: 610–626.

doi: 10.3164/jcbn.21-134

27 Bayır H, Anthonymuthu TS, Tyurina YY, *et al*. Achieving life through death: redox biology of lipid peroxidation in ferroptosis. *Cell Chem Biol* 2020; **27**: 387–408.
28 Cheng Z, Akatsuka S, Li GH, Mori K, Takahashi T, Toyokuni S. Ferroptosis-resistance determines high susceptibility of murine A/J strain to iron-induced renal carcinogenesis. *Cancer Sci* 2021. DOI: 10.1111/cas.15175
29 Pham-Huy LA, He H, Pham-Huy C. Free radicals, antioxidants in disease and health. *Int J Biomed Sci* 2008; **4**: 89–96.
30 Nakabeppu Y, Tsuchimoto D, Furuichi M, Sakumi K. The defense mechanisms in mammalian cells against oxidative damage in nucleic acids and their involvement in the suppression of mutagenesis and cell death. *Free Radic Res* 2004; **38**: 423–429.
31 Akatsuka S, Li GH, Kawaguchi S, *et al*. Augmented oxidative stress increases 8-oxoguanine preferentially in the transcriptionally active genomic regions. *Free Radic Res* 2020; **54**: 872–882.
32 Smith MR, Clark B, Lüdicke F, *et al*. Evaluation of the Tobacco Heating System 2.2. Part 1: Description of the system and the scientific assessment program. *Regul Toxicol Pharmacol* 2016; **81 Suppl 2**: S17–S26.
33 Chen C, Zhuang YL, Zhu SH. E-cigarette design preference and smoking cessation: a U.S. population study. *Am J Prev Med* 2016; **51**: 356–363.
34 Patel D, Davis KC, Cox S, *et al*. Reasons for current E-cigarette use among U.S. adults. *Prev Med* 2016; **93**: 14–20.
35 Uchiyama S, Noguchi M, Takagi N, *et al*. Simple determination of gaseous and particulate compounds generated from heated tobacco products. *Chem Res Toxicol* 2018; **31**: 585–593.
36 Bekki K, Inaba Y, Uchiyama S, Kunugita N. Comparison of chemicals in mainstream smoke in heat-not-burn tobacco and combustion cigarettes. *J UOEH* 2017; **39**: 201–207.
37 Wang G, Liu W, Song W. Toxicity assessment of electronic cigarettes. *Inhal Toxicol* 2019; **31**: 259–273.
38 Toyokuni S, Miyake N, Hiai H, *et al*. The monoclonal antibody specific for the 4-hydroxy-2-nonenal histidine adduct. *FEBS Lett* 1995; **359**: 189–191.
39 Ermakova YG, Bilan DS, Matlashov ME, *et al*. Red fluorescent genetically encoded indicator for intracellular hydrogen peroxide. *Nat Commun* 2014; **5**: 5222.
40 Linkermann A, Stockwell BR, Krautwald S, Anders HJ. Regulated cell death and inflammation: an auto-amplification loop causes organ failure. *Nat Rev Immunol* 2014; **14**: 759–767.
41 Hayden MS, Ghosh S. Regulation of NF-κB by TNF family cytokines. *Semin Immunol* 2014; **26**: 253–266.
42 Ling J, Kang Y, Zhao R, *et al*. KrasG12D-induced IKK2/β/NF-κB activation by IL-1α and p62 feedforward loops is required for development of pancreatic ductal adenocarcinoma. *Cancer Cell* 2012; **21**: 105–120.
43 MacNee W. Oxidative stress and lung inflammation in airways disease. *Eur J Pharmacol* 2001; **429**: 195–207.
44 MacKenzie EL, Iwasaki K, Tsuji Y. Intracellular iron transport and storage: from molecular mechanisms to health implications. *Antioxid Redox Signal* 2008; **10**: 997–1030.
45 Yanatori I, Richardson DR, Toyokuni S, Kishi F. The new role of poly (rC)-binding proteins as iron transport chaperones: proteins that could couple with inter-organelle interactions to safely traffic iron. *Biochim Biophys Acta Gen Subj* 2020; **1864**: 129685.
46 Toyokuni S, Kong Y, Cheng Z, *et al*. Carcinogenesis as side effects of iron and oxygen utilization: from the unveiled truth toward ultimate bioengineering. *Cancers (Basel)* 2020; **12**: 3320.
47 Dixon SJ, Lemberg KM, Lamprecht MR, *et al*. Ferroptosis: an iron-dependent form of nonapoptotic cell death. *Cell* 2012; **149**: 1060–1072.
48 Tang D, Kroemer G. Ferroptosis. *Curr Biol* 2020; **30**: R1292–R1297.
49 Tenopoulou M, Kurz T, Doulias PT, Galaris D, Brunk UT. Does the calcein-AM method assay the total cellular 'labile iron pool' or only a fraction of it? *Biochem J* 2007; **403**: 261–266.
50 Moscat J, Karin M, Diaz-Meco MT. p62 in cancer: signaling adaptor beyond autophagy. *Cell* 2016; **167**: 606–609.
51 Toyokuni S. The origin and future of oxidative stress pathology: from the recognition of carcinogenesis as an iron addiction with ferroptosisresistance to non-thermal plasma therapy. *Pathol Int* 2016; **66**: 245–259.
52 Zheng H, Jiang L, Tsuduki T, Conrad M, Toyokuni S. Embryonal erythropoiesis and aging exploit ferroptosis. *Redox Biol* 2021; **48**: 102175.
53 Fenton HJH. Oxidation of tartaric acid in presence of iron. *J Chem Soc* 1894; **65**: 899–910.
54 Kajiyama H, Utsumi F, Nakamura K, *et al*. Future perspective of strategic non-thermal plasma therapy for cancer treatment. *J Clin Biochem Nutr* 2017; **60**: 33–38.
55 Jiang L, Zheng H, Lyu Q, *et al*. Lysosomal nitric oxide determines transition from autophagy to ferroptosis after exposure to plasma-activated Ringer's lactate. *Redox Biol* 2021; **43**: 101989.
56 Winnicka L, Shenoy MA. EVALI and the pulmonary toxicity of electronic cigarettes: a review. *J Gen Intern Med* 2020; **35**: 2130–2135.